International Journal of Hydrogen Energy 81 (2024) 521–534

Contents lists available at ScienceDirect

International Journal of Hydrogen Energy

journal homepage: www.elsevier.com/locate/he

Separating hydrogen isotopologues via kinetic quantum sieving: Understanding important pore characteristics for an efficient separation

Massimo Mella [a,*], Andrea Tagliabue [a,b]

[a] Dipartimento di Scienza ed Alta Tecnologia, Università degli Studi dell'Insubria, via Valleggio 11, Como, 22100, Italy
[b] Dipartimento di Fisica, Università di Genova, Via Dodecaneso 33, Genoa, 16146, Italy

ARTICLE INFO

Keywords:
Hydrogen molecule
Isotopologues
Separation
Kinetic quantum sieving
Porous membranes

ABSTRACT

The potential performance of porous membranes in separating hydrogen isotopologues has been explored employing model systems and quanto-mechanical calculations including both zero-point energy and a numerically exact description of tunneling effects along the reaction coordinate. Membranes have been modeled as cylindrically pierced impenetrable wall, whereas diatomic molecules are described as dumbells composed of hard-sphere atoms. With the relative energetics of diatomics confined into cylindrical pores suggesting that differences in the adiabatic energy profiles between isotopologues for pore radii lower than 2.1 Å should favor transport of heavier species, we investigated the selectivity for the latter process when membranes are 2.0 Å thick. Chosen a pore radius, the results suggest that non-interacting pores represent the best compromise between selectivity and permeance, the addition of attraction between the membrane walls and molecular projectiles improving permeance while markedly depressing selectivity. A repulsive interaction with the pore inner surface, instead, reduced both properties. Finally, sieving molecules through a double membrane layer was found to marginally impact on the separation properties, which could be improved, at best, by 25% with a careful selection of the inter-membrane distance. Our results appear useful for the process of designing more effective sieving systems to separate di-deuterium molecules from its lighter counterparts.

1. Introduction

As nuclear, and occasionally chemical, properties may differ substantially between isotopes, their efficient separation or enrichment have represented an important endeavour in many field of science and technology. For the sake of exemplification, we mention the fissile properties of ^{235}U, ^{239}Pu, and ^{232}Th, the need for both ^{2}H and ^{3}H due to the hydrogen fusion reaction, the request for ^{3}He to be employed in neutron sensors, as well as the β^{+}–emitting properties ^{18}F. As for chemistry, ^{2}H and ^{3}H (i.e. D and T) stable or long-lived nature foster their use in the study of reaction mechanisms [1], as tracers to investigate the metabolite production and distribution of various substances in the environment and living bodies (*vide* [2,3] and references therein), or to help unravelling molecular structure via spectroscopic experiments [4].

Rivalling with the plethora of applications of pure isotopes, there is unfortunately the elevated cost of their purification, which is very often due to very similar physical or chemical properties. This fact forces one to use either extreme conditions (i.e. very low temperatures, as during cryogenic distillation of light elements [5]) or repeated application of the same process (as in the Girdler sulfide process [6]). It comes thus as no surprise the fact that alternatives to the currently available processes have been sought over the last few decades.

Due to our specific interest in the separation of hydrogen isotopologues, it is worth mentioning two important classes of approaches, namely chemical affinity quantum sieving (CAQS) and kinetic quantum sieving (KQS). While the former exploits differences in the interaction modalities (i.e. adsorption *loci* or groups) or in the relative energetics (e.g. adsorption energy) between molecules containing different isotopes, the latter make use of the differences in relative kinetics (i.e. diffusion or pore penetration) in order to set up processes (e.g. chromatography) capable of separating (e.g.) D_2 from H_2.

Notoriously, the two classes have specific advantages and disadvantages; for instance, strongly selective chemisorbing sites inside zeolites quickly saturate upon increasing gas pressure when attempting to exploit CAQS, while reaching the maximum KQS selectivity due to a preferential gate passage into a porous solid is *de facto* hampered by the accumulation and simultaneous desorption of both species [7–12].

In this work, we shall focus on studying specific characteristics of KQS mediated by the passage through monoatomic-thick porous membranes, graphdiyne [13–16] being one among the fews which have

* Corresponding author.
E-mail address: massimo.mella@uninsubria.it (M. Mella).

https://doi.org/10.1016/j.ijhydene.2024.07.055
Received 17 April 2024; Received in revised form 24 June 2024; Accepted 5 July 2024
Available online 25 July 2024

already been explored [17–21]. In the specific, we aim to investigate how the size and length of a pore pierced into a wall, the interaction modality of the latter and of the pore with the molecules (X_2, with X=H and D), and multi-membrane structures impact on the membrane separation capabilities. We do so by theoretical means, exploiting diffusion Monte Carlo (DMC) to build mono-dimensional anharmonic energy profiles, and numerical integration to compute transmission probabilities as a function of the kinetic energy.

Starting from an ideal system with only hard wall/hard sphere interactions, we build progressively more detailed models in the attempt of semi-quantitatively gauging the effects of the additional features on permeance and selectivity. The main aim of this work is thus to highlight general trends rather than gauging the performances of specific materials as previously done [13–15,17–23]. Compared to conceptually similar experimental analysis (*vide*, for instance, Refs. [12] and [24]), our approach better dissects contributions, as all details of our interaction models are under our precise control.

To summarize our results, we mention that hard-sphere/hard-wall type interaction-based systems seem to provide a very good balance between the two key properties, i.e. selectivity and permeance, these two quantities being, respectively, correlated and anti-correlated with pore size. Noteworthy, permeance may be increased compared to the latter cases by adding an attractive interaction between the molecular projectiles and the external membrane walls; this change, however, substantially lowers selectivity. Moreover, adding a repulsive potential inside the pore depresses, instead, both properties. Finally, layering in a parallel fashion two membranes with pore axes in coincidence slightly reduces permeances compared to single membrane cases; however, it bestows a distance-dependent oscillating behavior on it, with a wavelength that depends on the molecular mass. Consequently, the relative selectivity, which is defined as permeances ratio, oscillates between 75% and 126% of the one afforded by single membrane systems.

2. Models and methods

As indicated in the Introduction, we focus only on the most general features that both a porous membrane and diatomic molecules passing through pores in the latter may have, rather than attempting the description of a specific system. We do so to investigate what aspects ought to be considered important when it comes to separate hydrogen isotopologues. In doing this, we deviate from previous studies inasmuch as:

1. we included the description of the orientational degrees of freedom of the diatomic molecules (X_2), as considered important in the definition of the system energetics and dynamics when restraints can be placed by the system geometrical characteristics (compare, for instance, results obtained with a dumbbell-like and single atom representations of H_2 in Ref. [7]).
2. the transmission probability is obtained integrating the Schrödinger's Equation along the mono-dimensional transport coordinate energy profile, which is obtained by exactly computing (i.e. without invoking the harmonic approximation, e.g. see Refs. [19,20]) the ground state energy for the remaining four molecular degrees of freedom via a stochastic method (*vide infra* for more details) rather than by using basis set/grid based approaches (e.g. see Ref. [25–28]).

Specific details on the model systems and methodologies are further described in the following.

2.1. Model systems

The diatomic molecules H_2 and D_2 (in general, X_2) are bestowed with the characteristics:

1. of being dumbbell-like, with a fixed X–X distance equal to R_e = 0.767 Å (close to the vibrational averaged distance [29]);
2. of being composed by atoms with either an atomic mass of 1836.2 or 3669.6 in units of electron mass (m_e) for, respectively, H or D;
3. that each atom behaves as an impenetrable hard sphere of radius σ_{HS} = 1.11 Å (i.e. close to the tabulated van der Waals' radius of the hydrogen atom [30]).

With a similar spirit, an impenetrable wall with surfaces parallel to the XY plane of a set of orthogonal Cartesian axes was chosen as the simplest possible model representing a porous membrane, the surface being placed at $Z = -W_h$ or W_h (> 0). Noteworthy, it is the fact that choosing a value for W_h would implicitly define the type of material considered; in this work, we would consider only atomic-thick membranes (i.e. $W_h \simeq 1$ Å, *vide infra* for more details).

For the calculations required to obtain transmission probabilities, the wall is considered to be pierced by a cylindrical pore of radius R with its axis parallel to the Z one, and with its inner surface also being considered impenetrable as the membrane walls. Notice that this choice does not impact on the definition of the energy profile for a molecule passing through the pore itself, as each molecule must commit to a single pore once the distance between the center of mass (CoM) and the wall surface on the incoming side becomes lower than a threshold value that depends on the bond length and atom size (*vide infra*).

Fig. 1 provides a visual representation of the single pore, including explicit indications of possible positions and orientations for X_2 molecules. Apart from the excluded volume effects mentioned above, additional features that may be present in more realistic and specific cases are: (i) an additional repulsive interaction between the cylindrical (internal) pore surface and the hard sphere atoms when their CoM is inside the pore (akin to an electrostatic interaction between partial charges of the same sign); (ii) an attractive interaction between the external membrane surface and each of the atoms if their distance is below a threshold value, A_w. The latter characteristics can be easily added to the basic implementation of our chosen model in order to explore their impact on permeance and selectivity.

The complete modeling of the transport properties of a membrane necessitates also the calculation of permeance, the absolute value of the latter requiring the specification of the pores surface density. In this work, the cylindrical holes of radius R are positioned accordingly to a triangular lattice so that they are in tangential contact (i.e. the lattice translational vector is equal to 2R). With this choice, the pores are more densely packed compared to realistic cases such as graphdiyne [15], whose pore centers are more than 5 Å apart and characterized by a radius of roughly 0.4 Å. We would thus expect that our model suggested a higher permeance than any of materials so far investigated by theory.

A few qualitative considerations on the models' energetics can be easily made basing on the geometrical description of the systems provided above, assuming, for the time being, that only hard sphere/hard wall-like (i.e. excluded volume) interactions are present. Thus, making explicit reference to the positions and orientations of X_2 species in the left panel of Fig. 1, we notice that:

Case a. if the diatom center of mass is positioned so that $|Z_{CoM}| > W_h + R_e/2 + \sigma_{HS}$, X_2 is free to move along a plane parallel to XY and to assume uniformly distributed orientations of its bond axis. In this situation, there is no contribution to the system total energy from any of the four degrees of freedom (DoFs) not directly implicated in the molecular transport (i.e. X, Y, and the two spherical angles defining the molecular orientation with respect to the pore axis) as no constraints are imposed.

Case b. When $W_h + \sigma_{HS} < |Z_{CoM}| < W_h + R_e/2 + \sigma_{HS}$, the orientation with the bond axis parallel to the Z axis becomes forbidden unless an atom enters, at least partially, the pore. This constraint allows more or less wider "swings" of the second atom depending on how far inside the entrance the former is located, and it induces a non-zero contribution from the rotational kinetic energy. In this situation, mass-related quantum effects

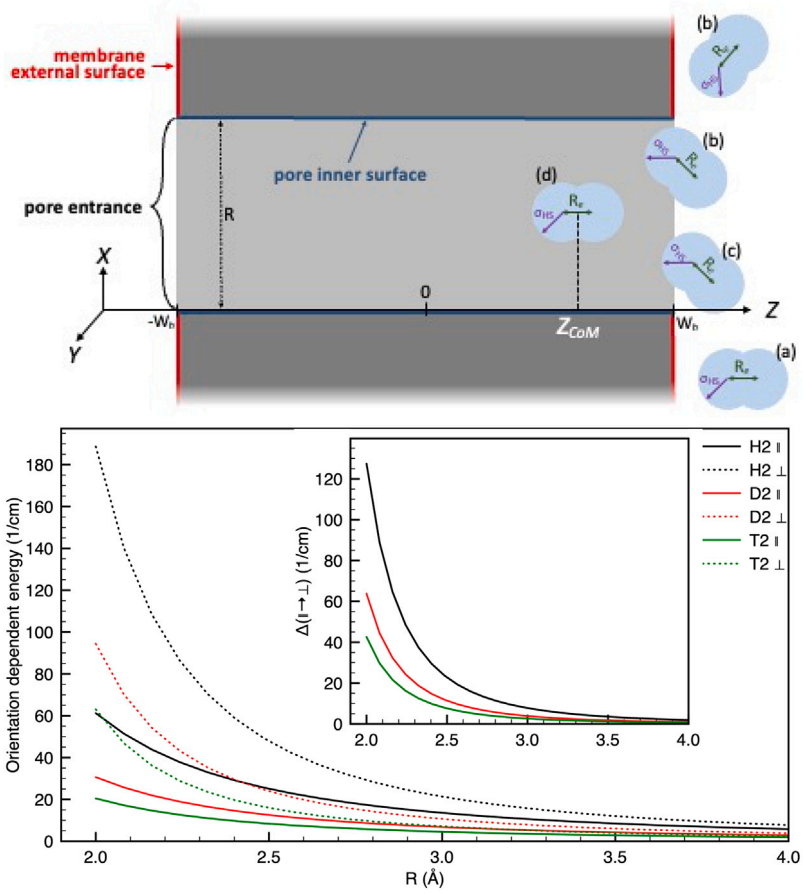

Fig. 1. Top: single pore portion of our model system, with the indication of its relevant geometrical characteristics and a few archetypical molecular configurations and orientations (*vide* main text for a discussion). Bottom: ground state quantum energy for hard sphere-like X_2 models inside an infinite pore as a function of pore radius R and assuming orientations parallel (∥) and perpendicular (⊥) to the pore axis. Results are obtained using Eq. (3) [31]. The inset shows the difference in energy between the two orientations. Despite being primarily interested in the separation between H_2 and D_2, we have also included results for T_2 for a general comparison on the mass effects.

should already become apparent, as the energy levels of the restrained angular motion depend on the molecule inertia moment. Notice, however, that molecular orientations parallel to the membrane surface remain possible, so that the transversal motion of the molecular CoM remains still non-quantized.

Case c. When $W_h < |Z_{CoM}| < W_h + \sigma_{HS}$, the amplitude of the orientational motion is progressively reduced upon decreasing $|Z_{CoM}|$, and the rotational kinetic energy component of the total energy is thus increased. Moreover, limitations are also placed on the motion parallel to the XY plane of the atom whose center is already inside the pore entrance, so that a contribution due to the restrained radial motion of the latter should also come into play. The latter would reach its maximum value once the atom center reaches the Z coordinate of the membrane surface ($+W_h$, if the molecule enters from the right hand side).

Case d. Once $|Z_{CoM}| \leq W_h$ (i.e. the molecule CoM enters the cylindrical pore), both its transversal motion and the molecule orientation experience their tightest restraints, and the kinetic energy assumes the maximum possible value. In the adiabatic approximation (*vide infra*) we wish to exploit, the latter would represent the effective barrier that the molecule has to overcome to reach the other side of the membrane, a barrier that is expected to be lower the heavier is the hydrogen isotopologue involved.

2.2. Methods

In this work, we aim to investigate the role played by several aspects of the interaction between diatomic species (H_2 and D_2) and the sieving membrane in order to better understand if and how it may be possible to improve the selectivity of the latter toward heavier isotopologues. Notice, however, that this task is far from trivial due to the number of DoFs of the system. In fact, even assuming that atoms composing the membrane are held rigid, and that the molecular vibration would remain in its ground state due to the limited amount of translational energy present, studying the quantum motion of X_2 system would require describing, at least, five DoFs. This is particularly true if one wished (as we do) to investigate also the impact of rotational motion and interaction anisotropy [7–10,32].

Albeit it is in principle possible, both time-dependent and time-independent approaches conserving all DoFs would be computationally very expensive [17,33]; this is especially true when attractive contributions to the overall interaction forces are included [15], as these impose long propagation times to simulate molecular escape from the attractive well. In principle, simplifications reducing the number of DoFs which need to be described are possible on the basis of an adiabatic separation between DoFs. However, properly choosing which DoFs require an explicit dynamical treatment is key in defining the quality of the approximated description one would eventually obtain.

As for the latter task, one may find guidance from recent works discussing the transport of H_2 molecules inside a carbon nanotube (CNT) [25] or through a porous membrane [15]. In the former, a comparison between a numerically exact diabatic treatment with its adiabatic counterpart, which explicitly describes only the motion along the axial transport coordinate over energy curves defined by the eigenvalues of the remaining DoFs, highlighted that the two approaches provide very similar results for the rate of transport at temperature below 120 K. This was also true for the flux-position correlation function

along the same coordinate despite the presence of energetic barriers of height roughly equal to 210 cm^{-1}. In addition, results in Ref. [15] indicated that permeances computed by using wave packets impinging perpendicularly on graphdiyne membrane closely follow the exact ones computed averaging over all possible incoming orientations, and they are also well reproduced by a description considering only the motion along the transport coordinate over a vibrationally averaged potential curve.

In view of the mentioned findings, we opted to follow an approach that exploits what just discussed and deals explicitly only with the rectilinear axial coordinate of the membrane cylindrical pores. The remaining four DoFs (i.e. the polar coordinates of the molecular center of mass inside the pore and the spherical angles indicating the molecular orientation with respect to the axis of the latter) were instead described as adiabatically separated and always remaining in their ground state. The latter choice may be easily justified basing on simple energetic considerations involving the gaps between ground and excited states for the four decoupled DoFs and the amount of translational kinetic energy along the transport coordinates allowed by thermal excitations, the latter being substantially lower than the state gaps for the species under investigation if $T \leq 100$ K.

Despite the adiabatic approximation invoked, the presence of attractive interactions between the membrane walls or pores may still require long integration times to converge the results if a time-dependent approach is used to estimate the kinetic constant of passing through a membrane pore. Thus, we opted for exploiting a time-independent approach previously introduced to deal with the deep tunneling regime and extreme resonating conditions [17,33]. This methods has, so far, being shown to provide accurate results with limited computational costs provided a one-dimensional (1D) energy curve is available to describe the reactive scattering process. If so, the integration of the time-independent Schrödinger Equation with the appropriate scattering initial conditions may be easily carried out by rewriting it as a system of coupled first order differential equations in both the real and imaginary parts of the wave function, the numerical solution of the latter having being obtained employing a standard fourth order Runge–Kutta approach [34].

Instead of using numerical or analytical basis functions to compute the adiabatic energy curve [25–28], we employed a variant of the diffusion Monte Carlo (DMC) method [35] explicitly tailored to deal with the holonomic constraints imposed to the internal coordinate of simple molecules [36–41]. In the latter approach, we fixed the diatomic CoM position along the pore axis and allowed DMC to sample the exact ground state wave function (ψ_0) for the remaining four DoFs. In short, we project out the contributions due to the system's excited states from any initial distributions of replicas (i.e. a set of 5D vectors $(x_{\mathrm{CoM}}, y_{\mathrm{CoM}}, z^{\mathrm{f}}_{\mathrm{CoM}}; \theta, \phi)$, with $z^{\mathrm{f}}_{\mathrm{CoM}}$ being the constrained position of the diatomic center of mass) simulating the evolution in imaginary time (i.e. $\tau = it$) imposed by the Wick-rotated Schrödinger Equation:

$$\mathcal{H}\psi_0 = \left[-\frac{\nabla^2_{\mathrm{CoM}}}{2m_{\mathrm{X_2}}} + \frac{\Lambda^2}{2I_{\mathrm{X_2}}} + \mathcal{V}_{\mathrm{ext}}(\mathbf{r}_{\mathrm{X_2}}, \Omega_{\mathrm{X_2}}) \right] \psi_0 = -\frac{\partial \psi_0}{\partial \tau} \tag{1}$$

via a sequence of alternated diffusion and branching step carried out as previously described in detail [36]. Here, Λ^2 is the total angular momentum operator, $I = \mu_{\mathrm{X_2}} r_e^2$ is the momentum of inertia ($\mu_{\mathrm{X_2}}$ being the reduced mass, and r_e the bond equilibrium distance), $\mathbf{r}_{\mathrm{X_2}}$ and $\Omega_{\mathrm{X_2}}$ being the position and orientation of the dimer, while $\mathcal{V}_{\mathrm{ext}}$ is the external potential representing the interaction with the membrane models. Albeit we shall discuss primarily separation between homo-dimers, the approach can easily be employed to investigate also hetero-dimers such as HD (*vide infra*) for specific results.

Importantly, we notice that the boundary conditions of the Schrödinger Equation describing the constrained diatomic motion inside the pore do not fulfill the analytical requirements (i.e. derivatives that vanish at the integration boundaries) for the average potential to be a correct estimator for the ground state energy, E_0. Thus, we employed the grow energy estimator, which is based on the change of the average weight of the configurations sampling ψ_0 by computing:

$$E_0 \simeq E_{\mathrm{grow}} = E_{\mathrm{ref}} - \delta\tau^{-1} \ln\left[N(\tau + \delta\tau)/N(\tau)\right] \tag{2}$$

where $N(\tau)$ is the sum of the statistical weight of the replicas, and E_{ref} is the reference energy chosen to avoid population "explosion" or collapse. The E_0 values obtained as a function of the position along the pore are subsequently used to generate a linear piece-wise representation for the ground state adiabatic energy curve to be employed in the calculation of transmission probabilities as a function of the projectile kinetic energy.

In the latter, we discretized the transport coordinate using a grid composed of 1000 points to cover an interval of 10 Å, at most; our preliminary tests indicated that our choice produced converged results, the computational effort requiring less than 30 s to obtain wave functions for 4000 kinetic energy values. Permeance values were obtained as clearly discussed for the graphdyine membrane [15] computing the thermal average of the transmission probabilities. Selectivities (S) were also estimated computing the ratio between the permeance of two isotopologues.

Finally, we mention that we also made use of classical Transition State Theory (c–TST) as a tool to rationalize results or to semi-quantitative predict general trends. In this work, our approach is based on the monomolecular c–TST analysis in Ref. [42], which can be recasted in the form $k_{\mathrm{TST}}(\mathrm{T}) = \frac{\langle Z_{\mathrm{CoM}} \rangle}{2V q_r} \int_R d\mathbf{x} \delta(Z_{\mathrm{CoM}}) e^{-\mathcal{V}_{\mathrm{ext}}(\mathbf{x})/(k_{\mathrm{B}}\mathrm{T})}$ by recognizing that the integral at the denominator over the CoM configuration space and molecular orientation is simply $V q_r$ (q_r is the rotational partition function and $\mathbf{x}$ is a point in reactant space). In our adiabatic model limited to the ground state of the transversal degrees of freedom, the remaining integral is simply $\exp[-E_0/(k_B T)]$ if one neglects the impact of thermal excitations; here, E_0 is the anharmonic ground state energy of a molecule enclosed into a pore.

3. Results and discussion

3.1. Geometry based considerations on the energetics of the model systems

To gauge the extent of the quantum effects in our model, we begin recalling that a point particle of mass equal to the H_2 molecule (i.e. $m = 2 \times 1836.2\, m_e$) and moving inside a circle of radius R (in Å) would have a ground state energy equal to

$$\mathrm{E}_0 \approx \frac{48.5}{\mathrm{R}^2} \tag{3}$$

in cm^{-1} [31]. If, instead, the molecules is bestowed with a size of its own (e.g. it behaves as a hard sphere of radius $\sigma_{\mathrm{HS}} < \mathrm{R}$) the quantity R should reflect the radial amplitude of motion (i.e. $R - \sigma_{\mathrm{HS}}$), so that E_0 would be higher than for the point-particle. In the case of a diatom, the situation is made slightly more complicated by the fact that the amplitude depends on the orientation, so that it is either $\mathrm{R} - \sigma_{\mathrm{HS}}$, if it is parallel to the pore axis, or $\mathrm{R} - (\mathrm{R}_e/2 + \sigma_{\mathrm{HS}})$, if it is perpendicular to it.

As a direct consequence of these observations, it becomes immediately apparent that being absorbed into a cylindrical pore should bias the molecular orientation favoring those parallel to the pore axis, at least when R is sufficiently small so that the energy difference between the two orientations becomes comparable with the gap between the ground and the first available excited state. As far as H_2 is concerned, such gap is around 356.7 cm^{-1}; it becomes 178.5 and 119.2 cm^{-1} for, respectively, D_2 and T_2. To understand when the latter effect ought to play a role, the bottom panel of Fig. 1 shows the difference in energy between parallel and perpendicular molecular orientations as function of R for the three isotopologues as computed via Eq. (3).

From Fig. 1, it is evident that:

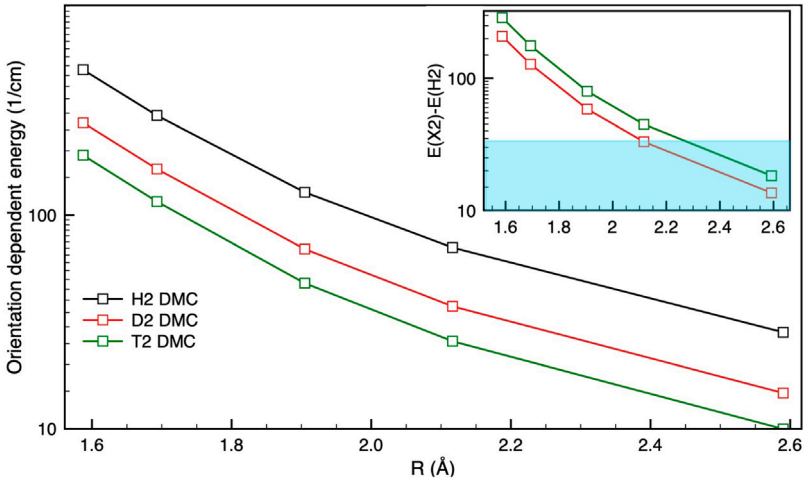

Fig. 2. Ground state energy (E_0) for the H_2, D_2, and T_2 model systems inside pores of radius R and with $W_h = \infty$. Statistical errors for E_0 are smaller than the symbols. The inset shows how the difference in E_0 between D_2, or T_2, and H_2 depends on R, the light blue shading indicating the values for which a selectivity lower than roughly 6 is obtained when the temperature is 20 K. This value is estimated by means of Transition State Theory without tunneling corrections, as indicated in the main text. (For interpretation of the references to color in this figure legend, the reader is referred to the web version of this article.)

1. Ground state energies increase upon increasing the confinement (i.e. decreasing R), E_0 for the perpendicular orientation growing more rapidly than E_0 for the parallel disposition. This indicates that lower transport rates ought to be expected upon decreasing the pore width.
2. The difference in E_0 between different isotopologues increases upon decreasing R for both orientations, so that the effective energy barriers due to the lateral confinement should favor more the passage of the heavier isotopologues the narrower the pore is.
3. For a chosen R value, the largest difference between the barrier heights for different isotopologues is found for the perpendicular orientations.

3.2. Diatomic molecules composed of hard-sphere atoms inside infinite hard-walled pores

To understand the general energetic behavior for the isotopologues inside a rigid pore, we employed DMC to compute the ground state energy (E_0) of the hard sphere dumbbell-like X_2 species inside infinitely long pores (i.e. $W_h = \infty$) of various radiuses R, the results being shown in Fig. 2 . As expected, E_0 decreases upon increasing the isotope mass for any chosen pore radius, while it monotonically increases upon decreasing R. Comparing with results in the bottom panel of Fig. 1, we also notice that E_0 results consistently sit between the energy curves for the two alternative orientations of each isotopologue with respect to the pore axis; a similar quantitative relationship is also clearly present between the rates at which E_0 increases, a finding suggesting, in turn, that molecules may assume a non-homogeneous distribution of orientations when in their ground state inside the rigid pore.

As for the absolute values of E_0, we notice that the effective barrier represented by the E_0 values at R = 2.6 Å may already be too small to induce an effective separation between isotopes unless the temperature of the gas mixture is very low. In fact, discounting the effect due to different masses on the average molecular speed and q_r of H_2 and D_2 for the time being, the c–TST approach discussed earlier predicts, in fact, a selectivity of roughly 2.9 at 20 K when R = 2.6 Å. In other words, our DMC E_0 values are already indicating that quite narrow pores may be needed to induce a substantial difference in the quantum energy of the transversal DoFs despite the negative impact that such choice may have on the overall flux though the membrane. To demonstrate that this may be the case, the inset in Fig. 2 shows the difference in E_0 between the two heavier isotopologues and H_2, the top of the light blue shading indicating the value for which the selectivity at 20 K (approximated as $S \simeq \exp\{-[E_0(X_2) - E_0(H_2)]/(k_B T)\}$), reaches the minimum industrially acceptable standard of 6 [43]. The intersections with the energy difference curves clearly indicate that one must have R ≃ 2.1 or 2.3 Å for, respectively, D_2 or T_2 to have a sufficiently higher preferential membrane permeation by the heavier species.

To further analyze the energetic aspects of absorbing a hard sphere-like X_2 species into a rigid pore, the total, translational, and rotational kinetic energy of the molecules has also been computed employing the finite field approach [44] that has previously been found useful to characterize adsorbed molecules [7–10,32]. The top panel of Fig. 3 presents the results obtained for the three species as a function of the pore radius. As expected, the total kinetic energy grows rapidly upon decreasing the pore radius. However, the only contribution to the total kinetic energy comes from the kinetic energy associated to the transversal motion of the molecule CoM when the pore is wide. Instead, the rotational component increases steeply only upon reducing the pore size below R = 1.9 Å, becoming roughly one third of the total kinetic energy when R ≃ 1.6 Å. It is thus clear that describing X_2 molecules as spherical objects may be rather inaccurate when the pore radius becomes comparable with half of the molecular bond length plus the van der Waals' radius of the atoms; the latter approximation is, in fact, likely to overestimate E_0. In turn, both permeance and selectivity would be underestimate due to, respectively, much higher barriers and smaller differences in kinetic energy for different isotopologues.

Albeit the increase in rotational kinetic energy shown in Fig. 3 upon decreasing the pore size is clearly due to the restraints imposed to the quantum rotational motion, it could also be interpreted in terms of free-rotor states as due to a forceful mixing between the $J = 0$ state with higher energy rotational states. The latter process is made possible by the symmetry breaking imposed by the pore walls, which couple together the CoM motion in the plane perpendicular to the pore axis with, particularly, the rotational states that orient the X_2 molecule axis parallel to the pore. In any case, a signature ought to be apparent in appropriate distributions sampled from ψ_0. Indeed, the distribution of the cosine for the relative orientation shown in the bottom panel of Fig. 3 evidences that the molecular axis is progressively oriented parallel to the pore one upon decreasing the pore size. We also notice that D_2 molecules should be more frequently oriented parallel to the pore than the lighter H_2, most likely due to the lower energy gap between rotational states. Indeed, the more marked ability of orienting parallel to the pore axis displayed by the heavier isotopologue represents a fundamental aspect impacting on the transmission probability though

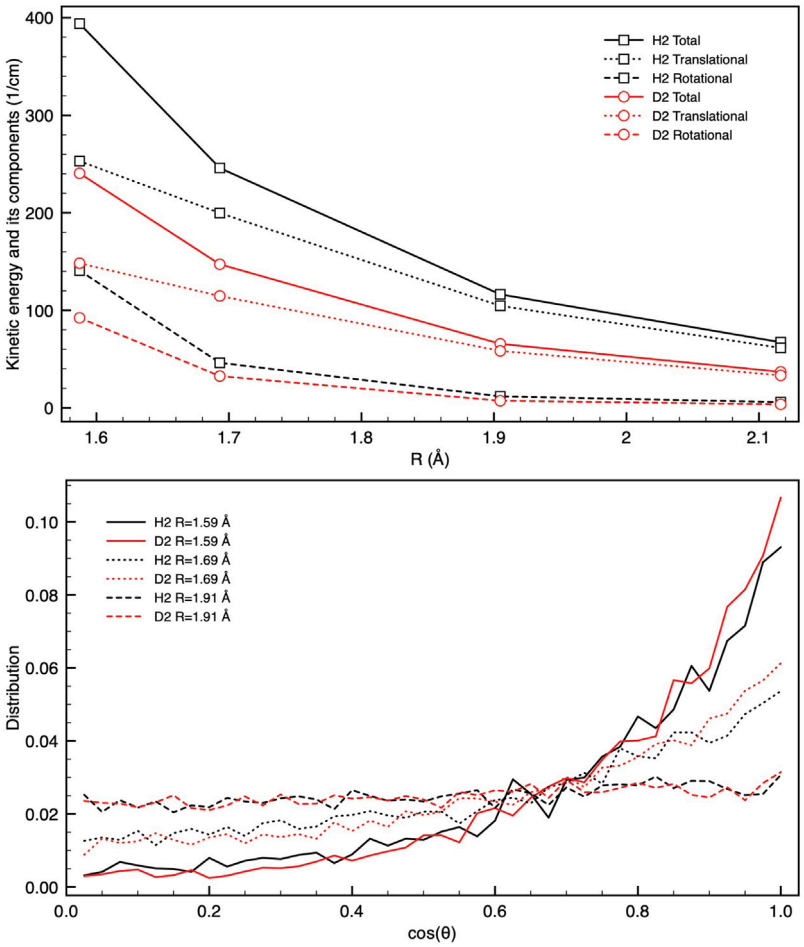

Fig. 3. (Top) Kinetic energy and its components for H_2 and D_2 model systems inside pores of radius R and with $W_h = \infty$. Standard errors for the energy components are $\simeq 5\,\mathrm{cm}^{-1}$. (Bottom) Probability distribution for the projection of the molecular axis orientation along the Z axis as obtained sampling the ground state wave function, ψ_0, for H_2 and D_2. For the sake of representation, we display only the positive values for the cosine.

the pore itself. In fact, the more a X_2 molecule is able to lie its axis parallel to the pore, the lower the effective size with respect to its motion along the XY plane would be. As a consequence, the range of radial motion that X_2 may afford would increase, while the kinetic energy associated with the latter should decrease. Thus, the energy barrier that is needed to be surmounted as a result of the restrained motion would be lower, making more likely for thermalized molecules to translocate from one side of the porous membrane to the other one.

3.3. X_2 molecules transport through short pores (i.e. $W_h = 1.06$ Å): hard-sphere atoms and hard-walled pores and membranes

As a reference systems against which gauging the impact of various aspects related to the interaction between X_2 molecules and the porous membrane devices, we have investigated the transport for the same system described in Section 3.2 (see Fig. 1) selecting $W_h = 1.06$ Å (i.e. 2 bohr), which is representative of the thickness usually found in carbon-based membranes such as pierced graphene [45–47] or graphdiyne [14,15,48,49]. The DMC results for the isotopologue energies as a function of the Z coordinate of the CoM along the pore axis, whose origin is placed midway through the pore itself, are shown in Fig. 4. For a comparison, we have also obtained the energy profile for HD in the narrowest pore (see Figure 1 in the Supporting Information), which sits between the ones for the two homo-dimers.

As expected the maximum energy value is located at $Z = 0$, and it agrees extremely well with the data shown in Fig. 2 for the ground state energy of the molecules inside an infinite pore. The profiles remain substantially flat until Z $\simeq$ 0.8 Å, a position after which they smoothly decrease (without intersecting) to the energy of molecules with unrestrained rotational and transversal DoFs. Complete freedom of motion is achieved when the CoM reaches $Z \simeq 2.5$ Å, the distance from the pore midpoint at which it is no longer possible for the rotating molecule to be in contact with the membrane surface or the pore edges. In other words, the energy of a molecule begins to be perturbed at a distance from the membrane surface comparable to the average molecular diameter.

As for the separation process itself, the straightforward application of c–TST concepts to the results shown in Fig. 4 would allow one to conclude that:

1. Assuming a limited importance of quantum tunneling in defining transport rates, heavier isotopologues ought to permeate more easily a membrane with sufficiently narrow pores (R $\leq$ 1.9 Å) and, hence, to be transported more rapidly from one side to the other when the temperature is below 100 K as the energy barrier to be surmounted decreases with the isotope mass. This conclusion is easily reached considering that the difference in barrier height when R = 1.9 Å is roughly 57 cm^{-1} (i.e. 90 K), so that the exponential part of the c–TST rate formula ought to substantially define the overall value of the transport rate ratio in favor of the heavier species despite the presence of the inverse dependence on the square root of the mass ratio due to the average velocity along Z_{CoM}.
2. Still within the assumption of a limited impact due to quantum tunneling effects, the rate of transport of X_2 species through

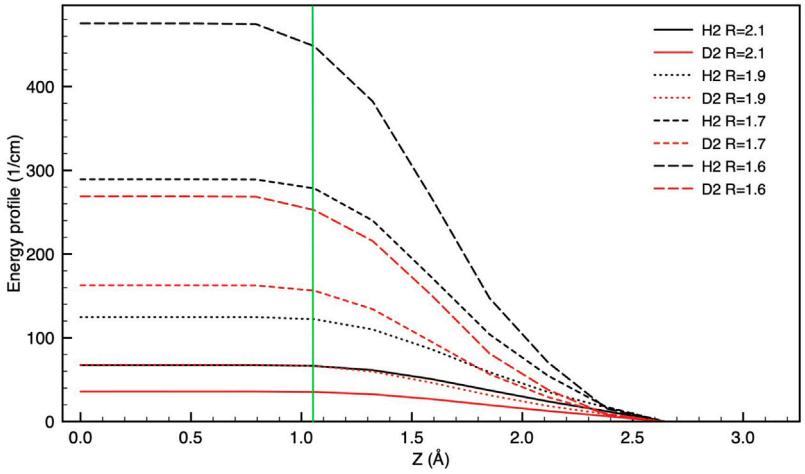

Fig. 4. Ground state energy profile of H_2 and D_2 molecules inside a membrane pore as a function of the CoM position along the pore axis for various R. The vertical green line represents the position of the pore rim. (For interpretation of the references to color in this figure legend, the reader is referred to the web version of this article.)

membrane pores should decrease very rapidly upon decreasing the pore radius due to the increase in barrier heights. Obviously, this impacts on the overall process rate, so that a compromise must be found between selectivity and overall process efficiency.

To bring quantitative support to the conclusions indicate above, we have computed the transmission probability as a function of the translational kinetic energy ($\mathcal{T}_R^{X_2}(E_{kin})$) for the various molecules and pore sizes accordingly to the approach discussed in the Methods section. This is the needed quantity to estimate gas permeance and, hence, selectivity as a function of the pore parameters.

The top panel of Fig. 5 presents $\mathcal{T}_R^{X_2}(E_{kin})$ results over a range of energy sufficiently ample to allow the Boltzmann's averaging and the calculation of permeance; $\mathcal{T}_{1.6}^{HD}(E_{kin})$ is also provided in Figure 1 of the Supporting Information. As it can be easily gauged, the transmission probability shows a rapid increase at energy values that markedly increase upon reducing the pore size (at fixed mass) or molecular mass (at fixed R), and also that it begins at lower energy than the associated barrier height (see Fig. 4 for a comparison). Both these trends are a clear indication that quantum tunneling effects should be expected to play a role in defining the low energy behavior. In other words, tunneling corrections ought to be included in the application of TST if one wished to accurately predict transfer rates at low temperatures [16,50]. The impact of quantum effects is also highlighted by:

1. an increase in $\mathcal{T}_R^{X_2}(E_{kin})$ that starts substantially earlier than the classical barrier height the lighter the molecule is, and that is less rapid for H_2 than D_2;
2. the dumped oscillatory behavior of $\mathcal{T}_R^{X_2}(E_{kin})$ that, after reaching nearly unit value, decreases to a local minimum roughly 5–12% lower, the height of the minima decreasing upon reducing the pore radius and molecular mass.

The latter finding is clearly a symptom of an "over the barrier reflection" phenomenon, which has already been theoretically well characterized in simpler model systems [31]. Worth a notice, this effect is far more apparent in the results of Fig. 5 than in the ones involving graphdiyne, a finding for which, at the present, we do not have a rationale.

Despite the evident contribution due to tunneling effects, transmission probabilities for D_2 remain larger than for H_2 at all energies apart in the 0–20 cm^{-1} range (i.e. 0–32 K), thus suggesting that D_2 permeance should be higher than H_2 one over a large temperature interval (roughly above 30 K); in turn, the selectivity toward D_2 ($S(D_2/H_2, T)$) should also be above unit. Indeed, the bottom panel of Fig. 5, which shows the selectivity and permeance for H_2 and D_2 as a function of the gas temperature, proves that this is the case. Similar comments could be made also for the separation between HD and H_2 basing on Figure 1 in the Supporting Information.

Discussing permeance first, we notice that it strongly depends on the temperature, increasing by orders of magnitude upon increasing the latter, an effect that is more evident the narrower the pore is. *De facto*, the Arrhenius-like plot of the permeance versus the temperature (i.e. the logarithm of permeance versus $1/T$) clearly shows that a linear-like behavior expected for activated processes is present in all cases apart for the passage of H_2 through the narrowest pore at temperatures below 17 K. The lack of temperature dependence present in that case can be easily interpreted as the indication that quantum effects have begun to play a key role in defining the molecular transport. Overall, the quantum results are in good agreements with what previously indicated basing on much simpler c–TST arguments, which could also predict that the permeance of the two isotopologues should converges toward a common limiting value upon increasing the temperature. Finally, we notice that the permeance reaches the industrially acceptable value of 20 GPU [43] at very low temperature in the vast majority of cases; for instance, a temperature of 50 K would be sufficient when D_2 is involved even for our narrowest pore.

Selectivities estimated by computing isotopic permeance ratios (Fig. 5) follow the trends expected on the basis of the permeance dependence on temperature and pore size. In fact, the selectivity increases upon decreasing the pore radius, while it decreases when the temperature is raised, exception made for $\mathcal{S}_{1.6\ Å}(D_2/H_2, T)$ below 12 K where the importance of the quantum tunneling in defining $\mathcal{T}_{1.6\ Å}^{X_2}(E_{kin})$ clearly emerges. As for $\mathcal{S}$ versus R behavior, we notice that only the narrowest pore appears able to induce a selectivity for the deuterium dimer above 6 (also an industrial standard) over a large portion of temperature interval explored, whereas temperatures below 74 K appears to be required already when R = 1.7 Å. Wider pores requires even lower system temperatures to ensure appropriate separation between the two isotopologues, so that it appears that some form of compromise should be reached between the rate of production of heavy isotopes, which increases upon increasing the pore width, and the total process costs. The latter are expected to raise upon lowering the temperature to enhance selectivity.

To deepen our understanding of the sieving process, we have also investigated the relative impact of molecular orientation on permeance and selectivity by freezing the relative orientation of the molecular axis either parallel or perpendicular to the pore axis; this is *de facto* equivalent to introducing in the channel two spherical objects with equal mass but different HS radius, the latter being, specifically, equal to 1.11 and 1.49 Å (see Section 2.1 for a more complete discussion).

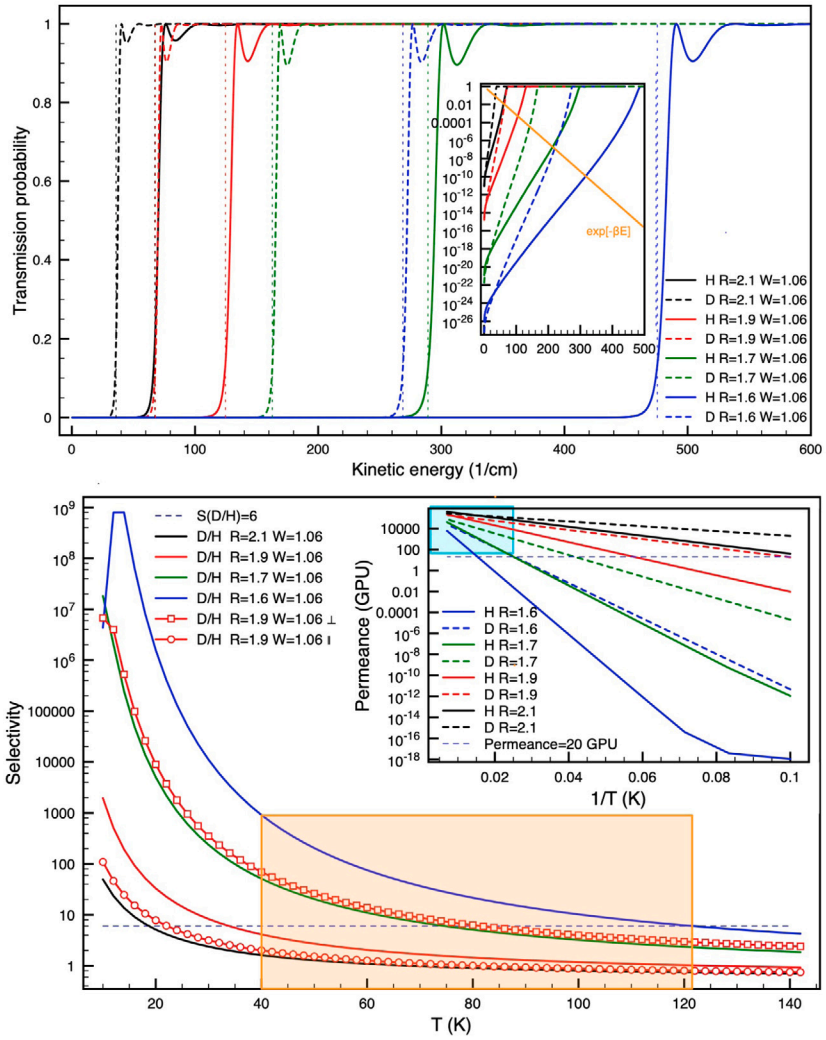

Fig. 5. (Top) Transmission probability through a rigid pore as a function of X_2 kinetic energy for various pore sizes. The inset shows the same data in a semi-logarithmic plot to highlight the low-energy tunneling behavior in the different cases. Vertical dotted lines indicate the maximum of the energy profile in Fig. 4 (i.e. the barrier) for the various cases. The orange curve shows the Boltzmann's exponential factor used to weight transmission probabilities during the calculation of transmission rates ($\beta = 1/(k_B T)$ with $T = 20$ K). (Bottom) Selectivity and permeance (inset) for H_2 and D_2 transport through a membrane pore as a function the gas temperature T, or its inverse 1/T, for various pore radiuses R. The horizontal dashed line indicate the minimum industrially viable selectivity. The light blue shading in the inset indicates the interval of temperature inside which the D_2 permeance though the narrowest pore exceeds 20 GPU; the same interval is also indicated in the main panel by the orange shading. (For interpretation of the references to color in this figure legend, the reader is referred to the web version of this article.)

$S_{1.9\ \text{Å}}(T)$ results obtained for the two orientations are thus presented in the bottom panel of Fig. 5. Importantly, we have chosen the pore with R = 1.9 Å as the barrier encountered by H_2 during its passage is already quite substantial compared to the thermal energy (roughly 125 cm^{-1}, see Fig. 4); yet, the chosen pore does not strongly bias the orientation of X_2 due to the mechanical constraints imposed (see the bottom panel of Fig. 3). From the results shown, it becomes apparent that S obtained with the DMC profiles is bracketed by the two extreme cases (as it should); it is however closer to the data obtained using the parallel orientation.

Even though it is not straightforward to decompose the DMC-based results in term of relative contributions for the two orientations, it nevertheless seems that the parallel one play the most important role in defining S. In turn, this suggests that there ought be a strong coupling between the radial position of the center of mass and the molecular orientation, so that the molecule tends to be parallel to the pore axis when its radial vibrational motion takes it close to the pore internal surface. The fact that the distribution of the azimuthal angle with respect to the pore axis does not display marked distortion is easily rationalized recalling that the radial distribution function must rapidly decrease toward zero upon increasing the distance from the axis itself, so that it should have a limited impact on the reorientation probability.

Finally, we have explored how permeance and selectivity depend on the membrane thickness by reducing W_h by 25% (i.e. using W_h = 0.79 Å). For the sake of space, we present the results for R = 1.9 and 2.1 Å in Figure 2 of the Supporting Information. In short, permeance increases minimally (25% is the maximum change predicted for the narrowest of the two pores) upon reducing the membrane thickness, the impact being weaker when R = 2.1 Å and the isotopologue heavier. As a consequence of the latter results, selectivity is reduced by roughly 25% when W_h = 0.79 Å and R = 1.9 Å compared to the thicker membranes case; the decrease is slightly less for the wider pore. The close similarity of transmission probabilities versus kinetic energy (*vide* bottom panel of Figure 2 of the Supporting Information) fully rationalize the limited changes in selectivity and permeance upon reducing the membrane thickness, especially if one notices that a earlier onset of transport through the pore is apparent for the thinner device.

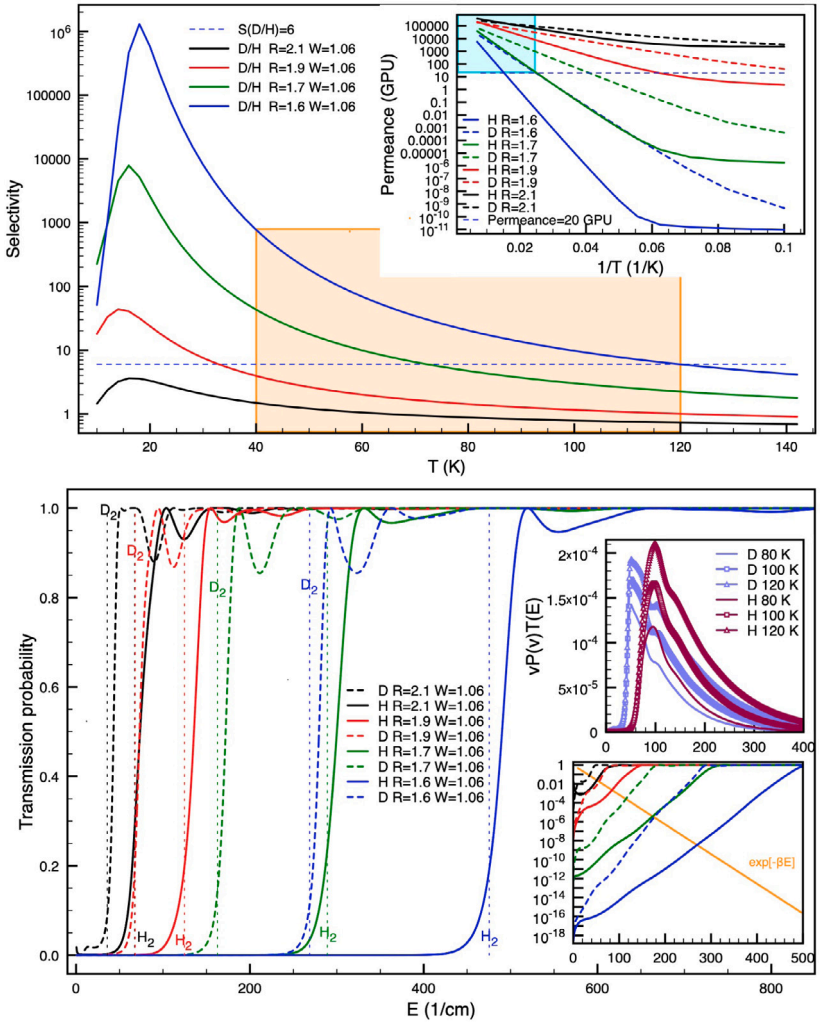

Fig. 6. (Top) Selectivity and permeance (inset) for H_2 and D_2 transport through a membrane pore as a function the gas temperature T, or its inverse 1/T, for various pore radiuses R. The wall external surface interacts attractively with X_2 via a square well potential of depth -120.7 cm^{-1} per atom. The light blue shading in the inset indicates the interval of temperature inside which the D_2 permeance though the narrowest pore exceeds 20 GPU; the same interval is also indicated in the main panel by the orange shading, with the upper limit being in coincidence with $S(T) = 6$, the industrially viable minimum selectivity. (Bottom) Transmission probability through the same pore system as a function of X_2 kinetic energy. The bottom right inset shows the same data in a semi-logarithmic plot to highlight the low-energy tunneling behavior in the different cases. Vertical dotted lines indicate the maximum of the energy profile in Fig. 4 (i.e. the barrier) for the various cases. The orange curve shows the Boltzmann's exponential factor used to weight transmission probabilities during the calculation of transmission rates ($\beta = 1/(k_B T)$ with $T = 20$ K) The top right inset shows the argument in the integral used to compute X_2 permeance when R = 2.1 Å for various temperatures. (For interpretation of the references to color in this figure legend, the reader is referred to the web version of this article.)

3.4. X_2 molecules transport through short pores: hard-sphere atoms and hard-walled membranes with attractive external interactions

In previous published contribution involving the theoretical study of porous materials for the separation of X_2 isotopologues, it was suggested that attractive interactions between the molecules and the wall or the pore rim may be beneficial for the overall separation process [19], as it may lead to a preferential accumulation of molecules close to the pore entrance. To shed some light on the possible impact of having the molecules being attracted by the membrane external wall and pore rims, we have thus added an attractive square well-like potential of width $\sigma_{HS} + 0.8$ Å, as measured from the membrane wall, and depth equal to -120.7 cm^{-1} per atom. The parameter values were selected in order to mimic the attractive potential present in the graphdiyne-X_2 case [15]. Fig. 6 shows the permeance and S results for pore radiuses spanning the range 1.6–2.1 Å.

We begin noticing that the presence of the attractive external well has a few major effects. First, permeances for both isotopologues are higher compared to the hard walled cases; the increase, however, depends on the operational temperature and molecular mass. In fact, we notice a limited increase at high temperatures, whereas a more marked one is seen when T is low. In the latter case, the increment is fivefold when D_2 impinges on the largest pore, while becomes 10^7 when H_2 is transferred through the narrowest pore. As a consequence, the range of temperatures inside which permeances are above the industrial requirement tends, thus, to increase somewhat, particularly for the two widest pores. Second, permeances appear to reach a limiting value (specific for each pore size) upon lowering the temperature instead than progressively decreasing, as previously evidenced. In fact, they remain orders of magnitude above the results described in the previous section. Third, and perhaps more importantly for our general goal, we notice a crossover at around 64 K between the permeances for H_2 and D_2 that was not present in Fig. 5 when R = 2.1 Å.

Seeking for possible causes of the quantitative changes induced by the external interaction, we notice that low-energy transmission probabilities are, indeed, higher when an attractive well is present outside the pore (*vide* bottom panel of Fig. 6 and top panel of Fig. 5). This may be due to the fact that:

1. X_2 projectiles impinge on the pore entrance with a kinetic energy that is much higher than the nominal value away from the wall,

as the attractive wall accelerates them. In turn, a higher energy means a less rapid decay of the wave function in the classically forbidden region and, thus, a higher overlap with the exit region on the other side of the wall (*vide* Figure 3 in the Supporting Information).
2. the width of the barrier is effectively reduced compared to the reference case due to the fact that when an atom is already penetrating the pore, the second may still be experiencing a stabilizing interaction with the wall (compare Fig. 4 with Figure 4 in the Supporting Information).

We also notice that there is a clear enhancement of the "over the barrier" reflection when an external attractive well is present, an this is demonstrated by the fact that the transmission probability does not reach unity as suddenly as it does in the hard-walled case once there is, nominally, a sufficient amount of kinetic energy to surmount it, and by the deeper local minima. However, the thermal average tends to decrease the impact of the latter effect, as indicated by the overall higher permeances.

The impact that an attractive well has on the molecular flow presents clear counterparts in how S changes in this circumstance, namely the fact that it decreases substantially compared to the cases discussed in Section 3.3. A marked non-monotonic behavior is also induced in the wider pores, due to an increase in relative importance of the tunneling in defining the selectivity upon decreasing the temperature. Finally, it is also evident that the widest pore may become selective toward the lightest isotopologue, the selectivity toward H_2 growing to roughly 1.5 upon increasing the temperature. With respect to the mentioned observations, a few factors that might play a role are:

1. a reduction of the effective barrier height experienced by the lightest isotopologue thanks to a higher zero point energy along the transversal modes;
2. a much higher tunneling probability for H_2, probably due to an effectively shorter pore (or effectively thinner barrier, as also suggested to justify the increased permeances);
3. a behavior that is becoming progressively more classical-like due to the higher velocities associated to the translational motion of the molecules, which are much more energetic.

Indeed, it is the latter effect that plays the key role, as clearly shown by the results for the transmission probability (Fig. 6) and the behavior of the integrand (see Equation 15 in Ref. [15], and the top right inset in the bottom panel of Fig. 6) that defines the permeances, the latter growing in height and raising its high energy tail due to the higher values of H_2 translational velocity. Besides, comparing the H_2 profile with D_2 one (see Figure 4 in the Supporting Information), it emerges that the barrier is higher for the former by more than 30 cm^{-1} (independently whether it is measured from the asymptote or from the profile minimum), and it is also wider by roughly 0.32 Å (as measured at the classical $E_{kin} = 0$ turning points).

3.5. X_2 molecules transport through short pores: hard-sphere atoms and hard-walled membranes with internal pore surface repulsion

In general, molecules inside short pores may experience energy barriers due to a repulsive interactions with the pore internal surface. This is mostly due to electrostatic and overlap/exchange interactions with the atoms or groups lining such regions. While one ought to expect an overall reduction in X_2 permeance compared to the simpler hard wall case, the effect on selectivity appears less straightforward to quantitatively gauge. In fact, the impact of tunneling, which should enhance H_2 permeance with respect to D_2 one especially at low energy, may be markedly reduced by the thermal averaging (see the discussion in Section 3.4).

The top panel of Fig. 7 presents the results for the hard-walled case plus inner pore repulsion. The latter has been introduced as a step-like potential of height 120 cm^{-1} acting on each atom when $-W_h \leq Z_{atom} \leq W_h$. A direct comparison with Fig. 5 indicates that the permeance for both isotopologues is reduced by the repulsive barrier, as expected. For instance, the new permeance value when R = 1.6 Å is 0.13 GPU for H_2 at 100 K, whereas it was 5.69 GPU in the original case. Similarly, the temperature at which D_2 permeance reaches the industrially acceptable value of 20 GPU becomes 72 K, while it was 47 K, originally. *De facto*, permeances for the pore with inner barrier are decreased by nearly three orders of magnitude at low temperature.

As for the effect on the selectivity, we notice that $S(T)$ is vastly decreased (by more than two orders of magnitude) in the low temperature regime by the presence of the potential barrier, while it quickly converges to quite similar values as the ones in Fig. 5 for temperatures above 40 K. Besides, there is a substantial difference in the trend of $S(T)$ for the wider pores, which evidently manifests a very fast decrease in selectivity lowering T below 20 K; in fact, the pores become selective toward the light isotopologue when the temperature is sufficiently low. The origin of this effect can be tracked comparing the transmission probability in the bottom panel of Fig. 7 with the ones in Fig. 5 (*vide* particularly the inset showing a semi-log plot). The former presents a much wider range of kinetic energy in which the H_2 permeance is higher than for D_2, the gap between the two quantities increasing upon decreasing the energy itself. It is also evident that, above 20 K (*vide* the plot of the Boltzmann's factor used for the thermal average at 20 K in the inset), the transmission probability for D_2 is already dominating the averages due to its much higher values for any pore width, so that all pores ought to return to be D_2–selective from that temperature onward.

As a last attempt to improve our understanding for simple "pore–in–wall" systems, we have also combined an external attractive well of identical size and depth as the one discussed in Section 3.4 to the repulsive pore case just presented. For the sake of easiness of reading, we report the results for R = 1.6 and 2.1 Å in Figure 5 of the Supporting Information; both permeance and selectivity behave as aspected basing on previously discussed results. In short, we notice that:

1. low temperature permeances are increased with respect to the repulsive pore case, as expected basing on Section 3.4, while they remain substantially lower than for the simpler hard-walled pores in Section 3.3;
2. selectivities are further decreased by the attractive well compared to the hard-walled and repulsive pore cases (*vide* Sections Section 3.3 and 3.4, respectively), especially at very low temperatures. *De facto*, the R = 2.1 Å pore with both attractive external wall and internally repulsive pores becomes progressively more selective toward H_2 below T = 24 K, a range of temperatures that seems, however, too low to be industrially exploited in a cost-effective manner.

3.6. X_2 molecules transport through short pores: molecules composed of hard-sphere atoms passing two parallel hard-walled porous membranes

As recent literature [17] suggested that placing two porous membranes in spatial series could improve selectivity, perhaps even without impacting too heavily on permeance, we have investigated such possibility for the same models employed in Section 3.3. The latter has, so far, provided the best overall performances in selectivity. Compared to the investigation exploring $^3He/^4He$ separation [17] , a situation in which both higher speeds and transmission probabilities for ^3He should facilitate its passage compared to ^4He if one excludes the contribution of transversal modes to the TS barrier [18,19], the same two effects are contrasted, in our case, by the adiabatic corrections included via the DMC simulations; this clearly favors the heavier D_2 [50].

As resonance states may appear impacting tunneling probabilities, we have explored the effect of varying the distance between walls, D, within the reasonable constraints imposed by the intercalation methods potentially employed to build such devices [51–56] . As for the specific

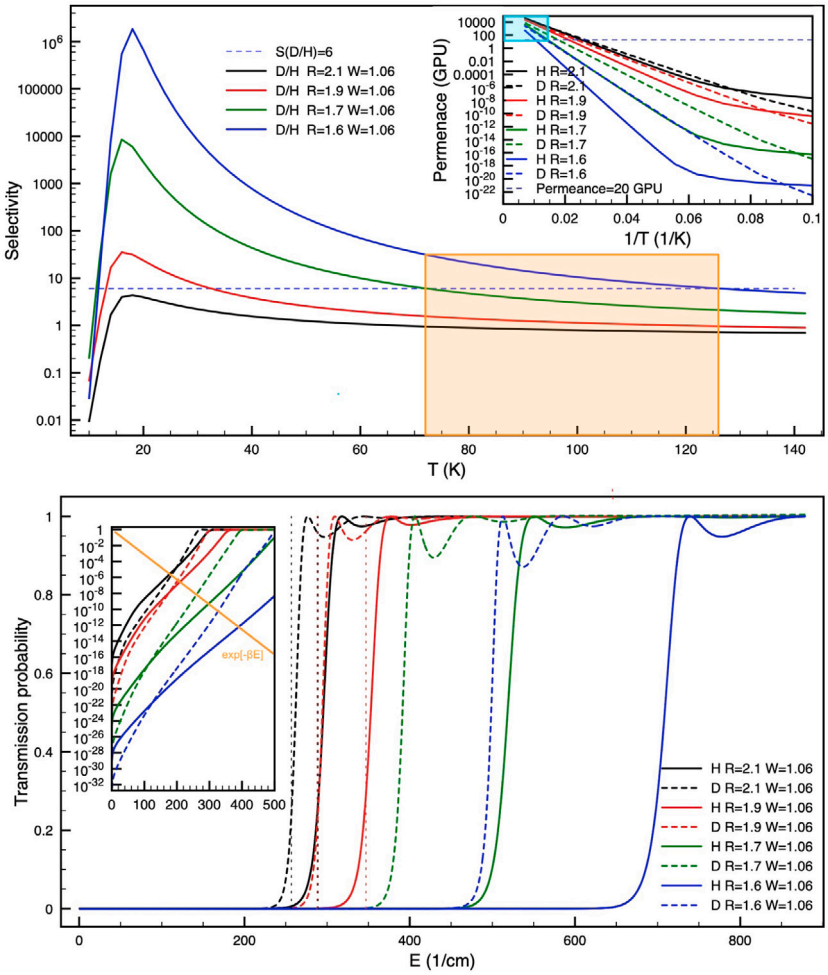

Fig. 7. (Top) Selectivity and permeance (inset) for H_2 and D_2 transport through a membrane pore as a function the gas temperature T, or its inverse 1/T, for various pore radiuses R. The pore inner surface interacts repulsively with X_2 via a square well potential of height 120 cm^{-1} per atom. The light blue shading in the inset indicates the interval of temperature inside which the D_2 permeance though the narrowest pore exceeds 20 GPU; the same interval is also indicated in the main panel by the orange shading. (Bottom) Transmission probability through the same pore system as a function of X_2 kinetic energy for various pore sizes. The bottom inset shows the same data in a semi-logarithmic plot to highlight the low-energy tunneling behavior in the different cases. Vertical dotted lines indicate the maximum of the energy profile in Fig. 4 (i.e. the barrier) for the various cases, which represents the effective barrier height also in this case (see top inset for the energy profiles in the R = 2.1 Å case). The orange curve shows the Boltzmann's exponential factor used to weight transmission probabilities during the calculation of transmission rates ($\beta = 1/(k_B T)$ with $T = 20$ K). (For interpretation of the references to color in this figure legend, the reader is referred to the web version of this article.)

details of the investigated pores, we have restricted ourselves to study the cases R = 1.6 and 1.9 Å, the rationale for this choice being the hope for a substantial improvement in the less selective case (R = 1.9 Å), and the necessity of gauging how much permeance may be reduced in the most selective (but least efficiently producing) case (R = 1.6 Å).

Relative selectivity and permeance results versus D are reported in Fig. 8 with respect to the single membrane sieving system; a subset of results regarding transmission probabilities are also presented in Figure 6 of the Supporting Information. We begin the discussion noticing that double membrane systems present relative permeances that present an oscillatory behavior as a function of D, and that are always lower than the single-membrane counterparts, with values increasing with both the projectile temperature and pore width. However, the reduction in permeance is never more than 25% of the single-membrane case, even in the worst possible case, i.e. H_2 sieved through pores 1.6 Å wide.

The oscillatory trend may be easily understood in term of the wave length associated to each projectile passing through the first pore, which, if naturally commensurate with the wall distance, may generate a constructive interference with the wave reflected by the second membrane. This would increase both the overlap and the energy similarity with the quasi-standing states of the projectiles contained between the membrane walls, so that the transmission probability may reach local maximum values [33,57,58]. The presence of the latter is, apparently, conserved by the thermal average. It is also interesting to notice that the relative position of maxima and minima for the two isotopomers is progressively modified by increasing D. This effect is easily understood if one notices that the relative value of the wave lengths for a specific value of the projectiles kinetic energy is given by $\frac{\lambda_{D_2}}{\lambda_{H_2}} = \sqrt{m_{H_2}/m_{D_2}} \simeq \sqrt{2}$, so that the alternation of maxima and minima in H_2 permeance requires a smaller wall displacements than for D_2.

Turning to selectivity, our results show that it can be both above or below the single membrane devices depending on D, the oscillation amplitude of the relative selectivity decreasing upon increasing the distance between the membranes or the pore width. It also decreases upon increasing the temperature, as it may have been expected as a consequence of the reduction in selectivity for the pores. The deviation of the selectivity with respect to the single membrane cases, however, never exceeds 26%, so that the advantage of making the sieving system more complicate appears limited, at best. This is, of course, valid for the specific geometry of our systems; it may, however, not be so if an offset is imposed to the axes of the pores on the two membranes. In this case, a partial randomization of the molecular motion might take place, as the ballistic motion of X_2 molecules would force them to bounce

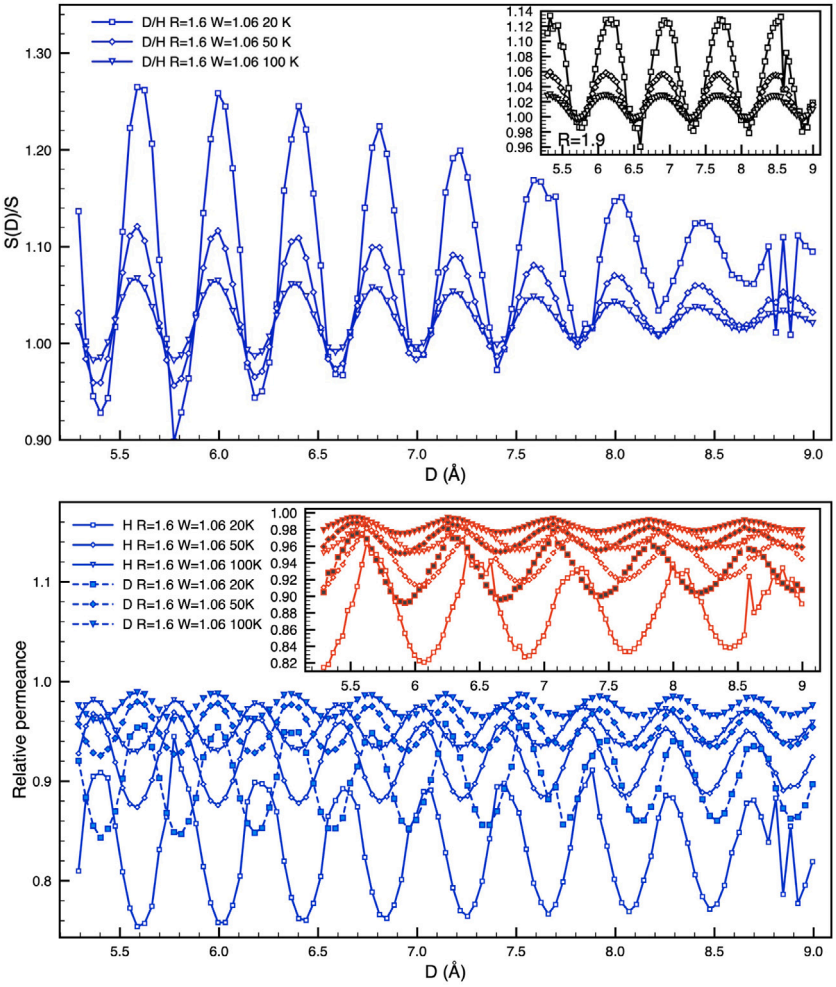

Fig. 8. (Top) Selectivity ratio for double- and single-membrane systems for hard sphere-like H_2, D_2 models for the transport through a membrane pore as a function of the membrane distance for three gas temperatures (20, 50, and 100 K) and two pore radiuses (R = 1.6 and, in the inset, 1.9 Å). (Bottom) Ratio between the double- and single-membrane systems permeance for the same cases shown in the upper panel. D_2 results are indicated by filled symbols.

backward. Of course, our 1D approach is not likely to correctly describe this process.

Comparing with the behavior of permeance versus D, it becomes also apparent that the higher selectivity shown by double-membrane devices compare to single-membrane ones is due, substantially, to the fact that minima in H_2 permeances are offset with respect to the same characteristics for D_2. This notwithstanding, one also notices that for distances in the range $5.3 \leq D \leq 7.2$ Å there is close matching between minima in H_2 permeances with maxima in D_2 ones, so that the relative selectivity is magnified, while they are progressively distanced upon increasing D. This latter aspect fully rationalize the decreasing amplitude in the oscillation of the relative selectivity (top panel of Fig. 8), as well as the progressive increase in the relative position between subsequent minima or maxima when $D > 7.2$ Å.

4. Conclusions

By choosing various potential energy models for the interaction between hydrogen isotopologues and membrane pores, we have studied how isotopic selectivity and global transport across the membrane is influenced by several characteristics such as pore size, interaction with the external membrane walls and the inner pore surface, or the double layering of membranes as a function of the system temperature. A summary of the discussed results is also provided in Figure 7 of the Supporting Information file, where we gathered together all data for a specific pore radius R. We have also minimally explored the process when HD is involved instead of D_2, as it seemed to conform to all the expectations one might form basing simply on its relative mass compared to H_2 and D_2.

Despite the fact that our energy models are simplified compared to what could be expected in more realistic systems (for instance, no vibrational motion is included in either the diatoms or the pore surface), they still contains many ingredients that are commonly present; as such, they can provide useful guidelines for the engineering of more effective and efficient devices to separate hydrogen isotopologues via KQS. In brief, it seems that the best, overall, performances in both selectivity and rate of production (permeances) are provided by the very ideal system we built as reference and to gain a few insights on the impact of geometrical features. In this, pores and membranes are described as hard-walled, while molecules are composed of hard-sphere atoms. In fact, adding attractive forces between external membrane walls and molecules increases permeance; it, however, negatively impacts on selectivity. We consider the latter to be a useful observation, which suggests to reduce the well depth as much as possible. Assuming that London's forces are the most intense at long distance, the goal could be reached reducing the polarizability of the atoms decorating the surfaces.

As for the inner pore surface, a repulsive interaction between the latter and molecular projectiles, instead, substantially depresses both permeance and selectivity, the decrease of S being primarily due to a more important role played by the light species tunneling.

Finally, layering in a parallel fashion two membranes only slightly impacts on permeances, depressing them by 25% at most, while an appropriate selection of the membrane distance appears to increase selectivity by 26%. In the end, it seems that the more "interactively neutral" the pore and the membrane are, the better are the performances in separating hydrogen isotopes.

Albeit our simplified models, and the connected results, have been specifically built to study transmission through membrane systems, nothing limits a semi-quantitative comparison with experimental results involving porous materials, provided the appropriate caveats are kept in mind. For instance, one may find useful the following considerations:

1. Hirscher et al. [12] have explored possible correlations between pore sizes and selectivity in quantum sieving. As such, they evidenced a maximum molar ratio of D_2/H_2 of roughly 7 at 19.5 K for COF–1, which affords a pore diameter of roughly 9 Å. The selectivity was, *de facto*, imputed to quantum confinement effects. If one compares results in Fig. 2, which suggest a difference in energy of 0.16 kJ/mol between D_2 and H_2 adsorbed into a pore 2.6 Å wide, with the isosteric heat of adsorption in COF-1 for the same molecules, one notices, instead, that a much higher energy difference (roughly 0.5 kJ/mol) is experimentally measured for a much wider pore. In our view, this difference suggests that what has been measured is not only connected to the translational confinement of the two molecules, but probably also to a much stronger interaction of D_2 with the inner surface of the material pores, most likely the oxygen atoms of the B_3O_3 moieties. This effect has already been evidenced [7–10] and it is related to both the higher total mass of D_2, and the larger inertia moment, bot responsible for lowering zero point energy and foster a more marked orientation ability. Albeit smaller than what predicted using the data in Fig. 2, the isosteric heat of adsorption into ZIF–8 appears, instead, as a legitimate quantum confinement effects, the difference with our model results being most likely due to the attractive interactions inside the porous material. This are expected to somewhat localize X_2 closer to the pore surfaces, possibly above the negatively charged imidazole rings with the diatoms pointing directly to their π system. Finally, the finding that ZIF–7 does not allow either of the isotopologues to enter is in agreement with the high amount of energy requested to enter our narrowest pore (i.e. roughly 190 and 220 K) compared to the thermal energy available in the experiments.
2. Even narrower strictures (2.52 Å) are present in MFU–4 [24], which prevent hydrogen molecules to enter (the estimated barrier is of roughly 800 cm^{-1}) unless a specific vibrational mode involving four chlorine atoms is thermally activated around 40 K. This finding, is again, in agreement with our results, as well as with the rapid raise in amount of adsorbed molecules upon increasing the temperature. In fact, Fig. 5 clearly shows that even a shift from 50 to 70 K may increase the rate of passage for D_2 by 9 times when R = 1.6 Å, a width that is probably comparable with the widest opening in MFU–4 generated by thermal activation. If one accepts a slightly wider width (i.e. R = 1.7 Å), the increase in adsorption rate is lower, becoming roughly equal to 4. As for the selectivities, our results are somewhat higher than the experiments, perhaps non-surprisingly as our model membrane systems do not accumulate passing molecules as porous materials tend to do, the net effect of which being to reduce the selectivity progressively due to preferential entering of H_2 at late exposure times. The dependence of S on T compares, instead, reasonably well, our R = 1.7 Å model showing a drop of a factor of 3 going from 50 to 70 K, compared to the experimental one of 2.1.

Improvements on the methodology and, hence, on the accuracy of the results are certainly possible. Here, we briefly mention the possibility of accounting explicitly for the nuclear spin of each isotopologues, as well as the possibility of including a few radial excited states moving beyond the adiabatic approximation. In principle, this would also allow exploring more complicate systems, such as the ones possessing cavities connected by pores. Also, the methodology could be employed to estimate diffusivity inside longer pores when the process requires thermal activation due to the presence of energetic barriers along the transport coordinate as suggested previously [25,26,28]. In fact, the limited computational cost involved in integrating the Schrödinger Equation along the reaction coordinate once the energy profile is obtained may allow one to estimate transition probabilities (or cumulative reaction probabilities, $N(E)$) for the jump over a few subsequent barriers, *de facto* facilitating the decorrelation between diffusion events. The determination of a few excited states for the diatom inside the pores would, however, be necessary to estimate the molecular partition function needed for the rate constant calculation. Work is underway to reach these goals.

CRediT authorship contribution statement

Massimo Mella: Writing – original draft, Supervision, Software, Methodology, Investigation, Formal analysis, Conceptualization. **Andrea Tagliabue:** Investigation.

Declaration of competing interest

The authors declare that they have no known competing financial interests or personal relationships that could have appeared to influence the work reported in this paper.

References

[1] Wiberg KB. The deuterium isotope effect. Chem Rev 1955;55(4):713–43. http://dx.doi.org/10.1021/cr50004a004.
[2] Polvoy I, Qin H, Flavell RR, Gordon J, Viswanath P, Sriram R, et al. Deuterium metabolic imaging–rediscovery of a spectroscopic tool. Metabolites 2021;11(9). http://dx.doi.org/10.3390/metabo11090570, URL https://www.mdpi.com/2218-1989/11/9/570.
[3] De Feyter HM, de Graaf RA. Deuterium metabolic imaging–back to the future. J Magn Reson 2021;326:106932. http://dx.doi.org/10.1016/j.jmr.2021.106932.
[4] Puzzarini C, Stanton J. Connections between the accuracy of rotational constants and equilibrium molecular structures. Phys Chem Chem Phys 2022;25. http://dx.doi.org/10.1039/D2CP04706C.
[5] Alekseev I, Arkhipov E, Bondarenko S, Fedorchenko O, Ganzha V, Ivshin K, et al. Cryogenic distillation facility for isotopic purification of protium and deuterium. Rev Sci Instrum 2015;86(12):125102. http://dx.doi.org/10.1063/1.4936413, arXiv:https://pubs.aip.org/aip/rsi/article-pdf/doi/10.1063/1.4936413/15843600/125102_1_online.pdf.
[6] Rae HK. Selecting heavy water processes. p. 1–26. http://dx.doi.org/10.1021/bk-1978-0068.ch001, Ch. 2. arXiv:http://pubs.acs.org/doi/pdf/10.1021/bk-1978-0068.ch001. URL http://pubs.acs.org/doi/abs/10.1021/bk-1978-0068.ch001.
[7] Mella M, Curotto E. Quest for inexpensive hydrogen isotopic fractionation: Do we need 2d quantum confining in porous materials or are rough surfaces enough? The case of ammonia nanoclusters. J Phys Chem A 2016;120(41):8148–59. http://dx.doi.org/10.1021/acs.jpca.6b08005.
[8] Curotto E, Mella M. Diffusion Monte Carlo simulations of gas phase and adsorbed D2-(H2)n clusters. J Chem Phys 2017;148(10):102315. http://dx.doi.org/10.1063/1.5000372, arXiv:https://pubs.aip.org/aip/jcp/article-pdf/doi/10.1063/1.5000372/15539999/102315_1_online.pdf.
[9] Mella M, Curotto E. Assessment of the effects of anisotropic interactions among hydrogen molecules and their isotopologues: A diffusion Monte Carlo investigation of gas phase and adsorbed clusters. J Phys Chem A 2017;121(26):5005–17. http://dx.doi.org/10.1021/acs.jpca.7b03768.
[10] Mella M, Curotto E. Quantum simulations of the hydrogen molecule on ammonia clusters. J Chem Phys 2013;139(12):124319. http://dx.doi.org/10.1063/1.4821648, URL http://scitation.aip.org/content/aip/journal/jcp/139/12/10.1063/1.4821648.
[11] Puricelli S, Bruno G, Gatti C, Ponti A, Mella M. Viability of hydrogen isotopes separation via heterolytic dissociation-driven chemical affinity quantum sieving on inexpensive alkali-earth oxides. Appl Surf Sci 2024;657:159596. http://dx.doi.org/10.1016/j.apsusc.2024.159596.

[12] Oh H, Park K, Kalidindi S, Fischer R, Hirscher M. Quantum cryo-sieving for hydrogen isotope separation in microporous frameworks: An experimental study on the correlation between effective quantum sieving and pore size. J Mater Chem A 2013;1(10):3244–8. http://dx.doi.org/10.1039/c3ta01544k.
[13] Poteryaeva V, Bubenchikov M. Separation of hydrogen isotopes using bi-layer membranes. Russian Phys J 2021;64(5):844–9. http://dx.doi.org/10.1007/s11182-021-02402-6.
[14] Gijón A, Campos-Martínez J, Hernández M. Wave packet calculations of the quantum transport of atoms through nanoporous membranes. J Phys Chem C 2017;121(36):19751–7. http://dx.doi.org/10.1021/acs.jpcc.7b04298.
[15] García-Arroyo E, Campos-Martínez J, Bartolomei M, Pirani F, Hernández MI. Molecular hydrogen isotope separation by a graphdiyne membrane: A quantum-mechanical study. Phys Chem Chem Phys 2022;24:15840–50. http://dx.doi.org/10.1039/D2CP01044E.
[16] Hernández MI, Bartolomei M, Campos-Martínez J. Transmission of helium isotopes through graphdiyne pores: Tunneling versus zero point energy effects. J Phys Chem A 2015;119(43):10743–9. http://dx.doi.org/10.1021/acs.jpca.5b08485, pMID: 26447561.
[17] Mandrà S, Schrier J, Ceotto M. Helium isotope enrichment by resonant tunneling through nanoporous graphene bilayers. J Phys Chem A 2014;118(33):6457–65. http://dx.doi.org/10.1021/jp502548r, pMID: 24854987.
[18] Hauser AW, Schwerdtfeger P. Nanoporous graphene membranes for efficient 3He/4He separation. J Phys Chem Lett 2012;3(2):209–13. http://dx.doi.org/10.1021/jz201504k.
[19] Hauser AW, Schrier J, Schwerdtfeger P. Helium tunneling through nitrogen-functionalized graphene pores: Pressure- and temperature-driven approaches to isotope separation. J Phys Chem C 2012;116(19):10819–27. http://dx.doi.org/10.1021/jp302498d.
[20] Qu Y, Li F, Zhao M. Efficient hydrogen isotopologues separation through a tunable potential barrier: The case of a C2N membrane. Sci Rep 2017;7(1):1483. http://dx.doi.org/10.1038/s41598-017-01488-8.
[21] Ning C, Zhang Y, Wang J, Gao H, Xiao C, Meng Z, et al. Theoretically designed two-dimensional γ–C4O as an effective gas separation membrane for hydrogen purification. Phys Chem Chem Phys 2020;22:19492–501. http://dx.doi.org/10.1039/D0CP02640A.
[22] Kumar AVA, Bhatia SK. Is kinetic molecular sieving of hydrogen isotopes feasible? J Phys Chem C 2008;112(30):11421–6. http://dx.doi.org/10.1021/jp8015358.
[23] Kumar AVA, Bhatia SK. Quantum effect induced reverse kinetic molecular sieving in microporous materials. Phys Rev Lett 2005;95:245901. http://dx.doi.org/10.1103/PhysRevLett.95.245901, URL http://link.aps.org/doi/10.1103/PhysRevLett.95.245901.
[24] Teufel J, Oh H, Hirscher M, Wahiduzzaman M, Zhechkov L, Kuc A, et al. Mfu-4 - a metal-organic framework for highly effective H2/D2 separation. Adv Mater 2013;25(4):635–9. http://dx.doi.org/10.1002/adma.201203383.
[25] Mondelo-Martell M, Huarte-Larrañaga F, Manthe U. Quantum dynamics of H2 in a carbon nanotube: Separation of time scales and resonance enhanced tunneling. J Chem Phys 2017;147(8):084103. http://dx.doi.org/10.1063/1.4995550, arXiv:https://pubs.aip.org/aip/jcp/article-pdf/doi/10.1063/1.4995550/15531504/084103_1_online.pdf.
[26] Mondelo-Martell M, Huarte-Larrañaga F. Diffusion of H2 and D2 confined in single-walled carbon nanotubes: Quantum dynamics and confinement effects. J Phys Chem A 2016;120(33):6501–12. http://dx.doi.org/10.1021/acs.jpca.6b00467, pMID: 27459476.
[27] Mondelo-Martell M, Huarte-Larrañaga F. 5D quantum dynamics of the H2@SWNT system: Quantitative study of the rotational-translational coupling. J Chem Phys 2015;142(8):084304. http://dx.doi.org/10.1063/1.4913293, arXiv:https://pubs.aip.org/aip/jcp/article-pdf/doi/10.1063/1.4913293/15491690/084304_1_online.pdf.
[28] Mondelo-Martell M, Huarte-Larrañaga F. Competition of quantum effects in H2/D2 sieving in narrow single-wall carbon nanotubes. Mol Phys 2021;119(14). http://dx.doi.org/10.1080/00268976.2021.1942277.
[29] Chang Y, An F, Chen Z, Luo Z, Zhao Y, Hu X, et al. Vibrationally excited molecular hydrogen production from the water photochemistry. Nature Commun 2021;12(1):6303. http://dx.doi.org/10.1038/s41467-021-26599-9.
[30] Rowland RS, Taylor R. Intermolecular nonbonded contact distances in organic crystal structures: Comparison with distances expected from Van Der Waals radii. J Phys Chem 1996;100(18):7384–91. http://dx.doi.org/10.1021/jp953141+.
[31] Johnson CSJ, Pedersen LG. Problems and solutions in quantum chemistry and physics. New York, NY: Dover Publications; 1986.
[32] Sheppleman Jr J, Smizaski G, Curotto E, Mella M. An analytical potential energy model for ammonia-H_2 from first principle. Chem Phys Lett 2012;535:49–55.
[33] Mandrà S, Valleau S, Ceotto M. Deep nuclear resonant tunneling thermal rate constant calculations. Int J Quantum Chem 2013;113(12):1722–34. http://dx.doi.org/10.1002/qua.24395, URL https://onlinelibrary.wiley.com/doi/abs/10.1002/qua.24395, arXiv:https://onlinelibrary.wiley.com/doi/pdf/10.1002/qua.24395.
[34] Press WH, Vetterling WT, Teukolsky SA, Flannery BP. Numerical recipes in FORTRAN. 2nd ed.. New York, NY: Cambridge University Press; 1994.
[35] Anderson JB. A random-walk simulation of the Schrödinger equation: H_3^+. J Chem Phys 1975;63(4):1499–503. http://dx.doi.org/10.1063/1.431514.
[36] Mella M. Higher order diffusion Monte Carlo propagators for linear rotors as diffusion on a sphere: Development and application to O_2@He_n. J Chem Phys 2011;135(11):114504. http://dx.doi.org/10.1063/1.3639190.
[37] Wolf S, Curotto E, Mella M. Quantum Monte Carlo methods for constrained systems. Int J Quantum Chem 2014;114(10):611–25. http://dx.doi.org/10.1002/qua.24647.
[38] Curotto E, Mella M. On the convergence of diffusion Monte Carlo in non-Euclidean spaces. I. Free diffusion. J Chem Phys 2015;142:114110.
[39] Curotto E, Mella M. On the convergence of diffusion Monte Carlo in non-Euclidean spaces. II. Diffusion with sources and sinks. J Chem Phys 2015;142:114111.
[40] Avilés M, Curotto E. Stereographic projection diffusion Monte Carlo (spdmc) algorithms for molecular condensed matter. J Phys Chem A 2007;111(13):2610–8.
[41] Curotto E, Freeman DL, Doll JD. A stereographic projection path integral study of the coupling between the orientation and the bending degrees of freedom of water. J Chem Phys 2008;128(20):204107. http://dx.doi.org/10.1063/1.2925681, URL http://link.aip.org/link/?JCP/128/204107/1.
[42] Mella M. Discretization error–free estimate of low temperature statistical dissociation rates in gas phase: Applications to Lennard-Jones clusters $X_{13-n}Y_n$ (n=0–3). J Chem Phys 2008;128(24):244515. http://dx.doi.org/10.1063/1.2937914.
[43] Zhu Z. Permeance should be used to characterize the productivity of a polymeric gas separation membrane. J Membr Sci 2006;281(1):754–6. http://dx.doi.org/10.1016/j.memsci.2006.04.040.
[44] Sandler P, Buch V, Clary DC. Calculation of expectation values of molecular systems using diffusion Monte Carlo in conjunction with the finite field method. J Chem Phys 1994;101(7):6353–5. http://dx.doi.org/10.1063/1.468388, URL http://scitation.aip.org/content/aip/journal/jcp/101/7/10.1063/1.468388.
[45] Dhali R, John C, Swathi R. Quantum transmission of he isotopes through crown ether-embedded graphene nanomeshes: An eckart potential approach. J Phys Chem A 2019;123(34):7499–506. http://dx.doi.org/10.1021/acs.jpca.9b06677.
[46] Qu Y, Li F, Zhou H, Zhao M. Highly efficient quantum sieving in porous graphene-like carbon nitride for light isotopes separation. Sci Rep 2016;6. http://dx.doi.org/10.1038/srep19952.
[47] Jiao Y, Du A, Hankel M, Smith S. Modelling carbon membranes for gas and isotope separation. Phys Chem Chem Phys 2013;15(14):4832–43. http://dx.doi.org/10.1039/c3cp44414g.
[48] Bhowmick S, Hernández MI, Campos-Martínez J, Suleimanov YV. Isotopic separation of helium through graphyne membranes: A ring polymer molecular dynamics study. Phys Chem Chem Phys 2021;23:18547–57. http://dx.doi.org/10.1039/D1CP02121D.
[49] Hernández M, Bartolomei M, Campos-Martínez J. Helium isotopes quantum sieving through graphtriyne membranes. Nanomaterials 2021;11(1):1–12. http://dx.doi.org/10.3390/nano11010073.
[50] Gao LG, Zhang RM, Xu X, Truhlar DG. Quantum effects on h2 diffusion in zeolite rho: Inverse kinetic isotope effect for sieving. J Am Chem Soc 2019;141(34):13635–42. http://dx.doi.org/10.1021/jacs.9b06506, pMID: 31362505.
[51] Sapkota I, Roundtree MA, Hall JH, Wang X-Q. Tunable band gap in gold intercalated graphene. Phys Chem Chem Phys 2012;14:15991–4. http://dx.doi.org/10.1039/C2CP43219F.
[52] Qi Y, Guo H, Hector LG, Timmons A. Threefold increase in the young's modulus of graphite negative electrode during lithium intercalation. J Electrochem Soc 2010;157(5):A558. http://dx.doi.org/10.1149/1.3327913.
[53] Huang Q, Chen X, Lin J, Li K, Jia Y, Liu J, et al. Preparation of quasi-free-standing graphene with a super large interlayer distance by methane intercalation. J Phys Chem C 2011;115(42):20538–45. http://dx.doi.org/10.1021/jp204723k.
[54] Sirisaksoontorn W, Adenuga AA, Remcho VT, Lerner MM. Preparation and characterization of a tetrabutylammonium graphite intercalation compound. J Am Chem Soc 2011;133(32):12436–8. http://dx.doi.org/10.1021/ja2053539, pMID: 21780799.
[55] Jin Z, Lu W, O'Neill KJ, Parilla PA, Simpson LJ, Kittrell C, et al. Nano-engineered spacing in graphene sheets for hydrogen storage. Chem Mater 2011;23(4):923–5. http://dx.doi.org/10.1021/cm1025188.
[56] Kim BH, Hong WG, Moon HR, Lee SM, Kim JM, Kang S, et al. Investigation on the existence of optimum interlayer distance for H2 uptake using pillared-graphene oxide. Int J Hydrog Energy 2012;37(19):14217–22. http://dx.doi.org/10.1016/j.ijhydene.2012.07.029, hYFUSEN.
[57] Neufeld O, Sharabi Y, Ben-Asher A, Moiseyev N. Calculating bound states resonances and scattering amplitudes for arbitrary 1d potentials with piecewise parabolas. J Phys A 2018;51(47):475301. http://dx.doi.org/10.1088/1751-8121/aae666.
[58] Dutt A, Kar S. Smooth double barriers in quantum mechanics. Am J Phys 2010;78(12):1352–60. http://dx.doi.org/10.1119/1.3481701, arXiv:https://pubs.aip.org/aapt/ajp/article-pdf/78/12/1352/12837581/1352_1_online.pdf.